Application of the Schwinger multichannel formulation to electron-impact excitation of the $b\ ^3\Sigma^+$ state of CO

Charles A. Weatherford
Department of Physics and Institute for Molecular Computations, Florida A&M University, Tallahassee, Florida 32307

Winifred M. Huo
NASA Ames Research Center, Mail Stop 230-3, Moffett Field, California 94035
(Received 8 December 1988; revised manuscript received 7 September 1989)

We report integral and differential cross sections for the electron-impact excitation of the $b\ ^3\Sigma^+$ state of CO using the Schwinger multichannel formulation. The calculations were carried out using a two-state approximation, with the incident electron energies in the range from 10.66 to 20 eV. We find four peaks in the inelastic cross section, centered at approximately 10.87, 11.6, 13.4, and 16.2 eV. The origins of the peak structures are discussed in terms of a partial-wave analysis, and comparison is made with experiment and theory where appropriate. We attribute the two sharp, low-energy (10.87 and 11.6 eV) peaks to the decay of $^2\Sigma^+$ core-excited Rydberg resonance states of CO^-. The two higher-energy peaks are broad and less well defined. The 13.4-eV peak is not clearly identifiable as a resonance, whereas the 16.2-eV peak in the inelastic cross section occurs as a result of a $^2\Sigma^+$ shape resonance in the elastic channel of the $b\ ^3\Sigma^+$ state. The magnitudes of the cross sections indicate that the $^2\Sigma^+$ symmetry is dominant for all four peaks. In all the resonances, we find more than one partial wave contributing at energies slightly shifted with respect to each other. The present calculation represents the first *ab initio* study of core-excited Rydberg resonances in electron-molecule scattering.

I. INTRODUCTION

Electronic excitations of molecules by low-energy electrons are receiving increasing attention by theoreticians and experimentalists.[1-4] The importance of these processes for atmospheric and plasma physics has long been known. In addition, electron-impact excitations have been used to induce population inversions in high-power electron beam and discharge pumped lasers[5] and to the study of adsorbate-substrate structures.[6] However, until recently, difficulties in performing the experiments and data analysis have inhibited experimental progress.[7] Similarly , the complicated nature of the projectile-target interaction potential (static, nonlocal exchange, polarization, correlation, multichannel) has prevented fast progress on the theoretical side.

The recent increased availability of vector computers has stimulated new theoretical progress. Four computational methods have demonstrated their capabilities of producing *ab initio* cross sections for electronically inelastic electron-molecule processes. A comparison of the four methods (the linear algebraic method,[8] the variational R-matrix method,[9] the Schwinger multichannel method,[10] and the complex Kohn method[11]) can be made by reviewing their simultaneous applications[8-11] to the excitation of the $b\ ^3\Sigma^+$ state of H_2. The Schwinger multichannel (SMC) formulation has been shown to be applicable to elastic scattering from such molecules as H_2, N_2, CH_4, and H_2O,[12-16] and to inelastic scattering from H_2, both in the gas phase,[17] and as an oriented molecule to simulate surface scattering.[18] Unlike some of the earlier *ab initio* methods,[19,20] the SMC method avoids dealing with the continuum wave function directly, and instead incorporates the scattering boundary conditions via a projected Lippmann-Schwinger equation. Also, exchange effects are included in an *ab initio* manner together with the correlation terms between the target orbitals and the continuum orbital. Thus the SMC method is able to treat the short- and long-range electron-molecule correlations from a completely *ab initio* point of view. Recently, the SMC method was employed to study the $^2\Pi_g$ shape resonance[21] and correlation effects[22] in electron-N_2 scattering. Therein, it was demonstrated that, within the context of the SMC formulation, the long-range electron-target polarization is associated with angular correlations and the short-range projectile-target correlation is associated with both angular and radial correlations.

The present study applied the SMC method to the calculation of the integral and differential cross sections for the transition $X\ ^1\Sigma^+ \rightarrow b\ ^3\Sigma^+$ in CO resulting from the impact of 10.66–20-eV electrons. The two relevant target states are included in the expansion of the 15-electron system. No closed channels are considered above the $b\ ^3\Sigma^+$ threshold. It should be noted that the transition of interest is optically forbidden and is thus governed by a short-range interaction. The present calculation fully accounts for the short-range exchange effect and approximates the electron-target correlation effects with the two-state treatment.

The $e+CO$ system is important for the modeling of plasmas,[23] the studies of CO adsorbed on surfaces,[24,25]

astrophysics of the interstellar medium,[26] and reentry physics.[27] A significant amount of experimental and theoretical data on the elastic cross section[2-4] exist in the literature, but the available data on inelastic processes[2,4] are sparse. The literature concerning resonances in electron-molecule scattering was summarized in 1973 in the review article by Schulz.[28] Specifically for the $b\ ^3\Sigma^+$ state, the only published data that we are aware of are the optical measurements of integrated cross sections by Skubenich,[29] the experiment of Newman, Zubek, and King,[30] using a low work function detector, the experimental relative total cross-section measurements of Polley and Bailey,[31] the experimental differential cross sections at 20 eV measured by Trajmar, Williams, and Cartwright,[32] the recent unpublished experimental results of Allan[33] using a trochoidal electron spectrometer, the semiempirical integral cross sections of Sawada, Sellin, and Green[34] and the Born calculations of Chung and Lin.[35] It should be noted that the first-order Born theory of Chung and Lin is not capable of predicting resonance behavior and the agreement between theory and experiment is not good. Calculations on this system using an up-to-date technique are warranted. Also, the $b\ ^3\Sigma^+$ state, a Rydberg $3s$ state, is the lowest Rydberg state of CO. A study of this system will serve as an example of electron-impact excitation of molecular Rydberg levels.

The present work explores the resonance structures above the $b\ ^3\Sigma^+$ threshold. We analyze the resonance structure by performing a partial-wave decomposition and establish the resonance positions based on the typical discontinuous behavior in the K-matrix elements as well as the π radian change in the partial-wave eigenphases. This resonance behavior will, in the process of the discussion, be related to the concept of core-excited resonances and the "grandparent" model of resonances.[28] To relate our results to the formation of the negative ion, we also carried out bound-state calculations on the $(5\sigma)(3s\sigma)^2$ core-excited Rydberg state of CO^-, and found the position agrees well with our low-energy resonance positions, but, due to the lack of proper correlation, it is slightly shifted to a higher energy from experiment. In Sec. II, we present a short discussion of the theory. In Sec. III, the computational procedure and results are presented. Finally, in Sec. IV, we present our conclusions.

II. THEORY

Detailed descriptions of the SMC formulation have been given previously.[12,13] To facilitate subsequent discussions of the computational procedure and results, we give a brief review of the working equations here. Let $\Psi_n^{(+)}$ be the total $(N+1)$-particle antisymmetrized wave function with incoming-plane-wave and outgoing-wave boundary conditions for the nth channel. A projected Lippman-Schwinger equation for $\Psi_n^{(+)}$ is

$$P\Psi_n^{(+)}=S_n+G_P^{(+)}V\Psi_n^{(+)} . \tag{1}$$

The projection operator P defines the open-channel space in terms of the eigenfunctions Φ_m of the target Hamiltonian H_N,

$$P=\sum_{m=1}^{M}|\Phi_M(1,2,\ldots,N)\rangle\langle\Phi_m(1,2,\ldots,N)| , \tag{2}$$

and

$$H_N|\Phi_m\rangle=E_m|\Phi_m\rangle . \tag{3}$$

The open channels are associated with those target states with energy E_m less than $\mathcal{E}$, the total energy of the (electron plus molecule) system. In Eq. (2) P is defined in the N-electron space instead of $(N+1)$-electron space as in the Feshbach formalism.[36] Also S_n, in Eq. (1), is the solution of the unperturbed Hamiltonian H_N+T_{N+1} and is given by

$$S_n=\sqrt{k_n/(2\pi)^3}\exp(i\mathbf{k}_n\cdot\mathbf{r}_{N+1})\Phi_n . \tag{4}$$

The interaction potential V between the incident electron and the target is

$$V=\sum_{i=1}^{N}\frac{1}{|\mathbf{r}_i-\mathbf{r}_{N+1}|}-\sum_a\frac{Z_a}{|\mathbf{R}_a-\mathbf{r}_{N+1}|} . \tag{5}$$

The outgoing-wave Green's function $G_P^{(+)}$, defined in the open-channel space, is given by

$$G_P^{(+)}=-\frac{1}{2\pi}\sum_{m=1}^{M}|\Phi_m\rangle\frac{\exp(ik_m|\mathbf{r}_{N+1}-\mathbf{r}'_{N+1})}{|\mathbf{r}_{N+1}-\mathbf{r}'_{N+1}|}\langle\Phi_m| . \tag{6}$$

To obtain a complete equation for Ψ_n, we must recover the unprojected component of Eq. (1). This is done by rearranging the Schrödinger equation to yield

$$[\hat{H}-a(P\hat{H}+\hat{H}P)]\Psi_n^{(+)}=a(VP-PV)\Psi_n^{(+)} , \tag{7}$$

where $\hat{H}=\mathcal{E}-H_{N+1}$. The value of a is determined as in Ref. 12. The above equation can be used to introduce the closed channels[14,21] without defining the closed-channel Green's function, which would require the inclusion of the target continuum states. Takatsuka and McKoy[12,13] have shown that a complete equation for $\Psi_n^{(+)}$ is given by

$$A^{(+)}\Psi_n^{(+)}=VS_n , \tag{8}$$

with

$$A^{(+)}=\tfrac{1}{2}(PV+VP)-VG_P^{(+)}V+\frac{1}{N+1}\left[\hat{H}-\frac{N+1}{2}(P\hat{H}+\hat{H}P)\right] . \tag{9}$$

Based on the fractional form of Schwinger's variational principle, the fixed-nuclei T matrix is expressed as

$$T_{mn}=\frac{\langle S_m|V|\Psi_n^{(+)}\rangle\langle\Psi_m^{(-)}|V|S_n\rangle}{\langle\Psi_m^{(-)}|A^{(+)}|\Psi_n^{(+)}\rangle} . \tag{10}$$

The above quantity is calculated in the molecular frame[37] using the fixed-nuclei approximation. It provides an expression for the body-frame T matrix for molecules of arbitrary geometry. The procedure for obtaining the physical scattering cross sections by a transformation to the laboratory frame and averaging over molecular orienta-

tion is described elsewhere.[38]

Equation (10) summarizes the multichannel formulation of electron-molecule collisions. This formulation has several important practical features. For example, all matrix elements in the variational expression given by Eq. (10), except those of $VG_P^{(+)}V$, can be evaluated analytically provided the trial scattering wave function is expanded in a basis of Gaussian functions and plane waves. If an approximate closure relation using Gaussian functions is inserted around $G_P^{(+)}$, then the matrix elements of $VG_P^{(+)}V$ can also be evaluated analytically, i.e.,

$$\langle \Psi_m^{(-)}|VG_P^{(+)}V|\Psi_n^{(+)}\rangle \simeq \sum_{\gamma,\delta} \rangle\Psi_m^{(-)}|V|\gamma\rangle\langle\gamma|G_P^{(+)}|\delta\rangle\langle\gamma|V|\Psi_n^{(+)}\rangle \ . \quad (11)$$

This method is termed the "α-insertion" technique. In addition, it has been shown that the contribution from the residue of $\langle \Psi_m^{(-)}|VG_P^{(+)}V|\Psi_n^{(+)}\rangle$ can be obtained in analytical form[21] and only the principal-value contribution to this matrix element needs to be evaluated by the method of Eq. (11). This is called the "k-insertion" technique. This technique is particularly useful because the residue contribution in Eq. (11) is often the dominant one. It has also been shown[21] that the unitarity of the calculated S matrix is determined entirely by the on-shell contribution. Thus the S matrix from k-insertion calculations has almost perfect unitarity. All our final production calculations were carried out using this technique. Possible insertion errors in the calculation of the principal-value contribution are estimated based on the following argument. Major contributions to the principal-value integral also comes from the vicinity of the poles of the Green's function. The error in representing the principal-value contribution should be related to the error in representing the residue using the α-insertion technique. Thus we routinely compare the results of k and α insertions to judge the completeness of the insertion basis.

In using partial-wave analysis to locate resonance structures, we use both the discontinuity of the K matrix and the sharp increase of the partial eigenphases over π radians as distinct resonance signatures. It may be noted that the SMC calculation directly produces T matrices. Both the K matrix and the eigenphases of the S matrix are deduced from the T matrix. A comparison of the two quantities serves as an internal consistency check for the computation.

III. COMPUTATIONAL PROCEDURE AND RESULTS

All calculations were carried out in the two-state approximation with the ground state of CO represented by self-consistent-field (SCF) wave function and the $b\,^3\Sigma^+$ state by an IVO (improved-virtual-orbital) wave function.[39] The NASA Ames SCF code was used for the target calculations. Both the target (N-particle) wave functions and the scattering [$(N+1)$-particle] wave functions were represented by a basis of Cartesian Gaussians. Table I presents the basis set used in our final calculations. This will be referred to as basis set A. We started with the uncontracted $9s5p$ set of Huzinaga[40] at the nuclei and added two diffuse s and p functions. In addition, set A also contains $3s3p1d$ Gaussians at the center of mass (c.m.). The diffuse s, p, and d functions serve to describe the continuum electron as well as the Rydberg character of the excited target state. This basis set is considerably more extensive than the set used by Chung and Lin[35] in their nonunitarized Born calculations. The ground state SCF energy determined using set A is $-112.736\,01$ hartrees, and the IVO excitation energy is 0.391 hartrees (10.65 eV). The corresponding experimental values[41] are -113.377 and 0.382 hartrees (10.40 eV). The calculated dipole moment for the ground state is -0.220 a.u. and for the $b\,^3\Sigma^+$ state, $+0.888$ a.u. The experimental value for the ground-state dipole moment is $+0.044$ a.u. No experimental data is available for the di-

TABLE I. Gaussian basis set[a] (A) used in the representation of $\Psi_n^{(+)}$ and $G_P^{(+)}$.

Center and type	Exponent (α)
C,11s	5240.635, 782.2848, 178.3508, 50.815 94, 16.823 56, 6.175 776, 2.418 049, 0.5119, 0.156 59, 0.05, 0.02
C,7p	18.8418, 4.159 24, 1.206 71, 0.385 54, 0.121 94, 0.045, 0.01
O,11s	10 662.28, 1599.71, 364.7253, 103.6518, 33.905 81, 12.287 47, 4.756 803, 1.004 271, 0.300 686, 0.1, 0.03
O,7p	34.856 46, 7.843 131, 2.308 269, 0.723 164, 0.214 882, 0.06, 0.2
Center of mass	
3s	0.01, 0.003
$3p_x, 3p_y$	0.09, 0.03, 0.010
$1d_{xx}, 1d_{yy}, 1d_{zz}$	
$1d_{xz}, 1d_{yz}$	0.80

[a] $\chi_{lmn}^{(\alpha)} = N_{lmn}(x-A_x)^l(y-A_y)^m(z-A_z)^n e^{-\alpha|\mathbf{r}-\mathbf{A}|^2}$

pole moment of the excited state. The sign error in the SCF dipole moment for the ground state is well documented.[42] We note that the calculated dipole moment for the b state is considerably larger than the ground state.

The Schwinger scattering calculations were performed with the NASA Ames SMC code.[43] Table II presents the SMC elastic integral cross sections for the ground state, and the inelastic integral cross sections for the $b\,^3\Sigma^+$ state, at incident electron energies between 10.66 and 20 eV. Since the elastic cross sections were calculated in the fixed nuclei approximation, they correspond approximately to electronically and vibrationally elastic but rotationally unresolved measurements, with the additional assumption that the rotational excitation energy is zero. Because CO is a polar molecule, the long-range electron-dipole potential leads to a slow fall off of the elastic T-matrix elements for large l. The large-l values contribute predominantly to the forward scattering angles in the elastic cross section. In the present calculation, only low-order angular momentum waves, with maximum $l=6$, were included in the partial-wave expansion. Previous calculations[16] on elastic scattering of H_2O showed that, in the energy range under consideration, such an approximation can provide differential cross sections in good agreement with experiment as long as the scattering angle is larger than 30°. Since the dipole moment of the ground state of CO is much smaller than H_2O, the argument should be more applicable in the present case. In comparing integral cross sections, we have made an additional approximation that the improper treatment of the forward scattering cross section has only minor effects on this quantity.

We present in Fig. 1 the elastic differential cross sections at 20 eV (between 30° and 180°) from the present calculation using k insertion, and the experimental data of Tanaka, Srivastava, and Chutjian[44] and Nickel.[45] General agreement is found between theory and experiment, except in the forward direction. The deviation at angles less than 30° is due to the use of low-order angular momentum waves used in the present calculation. For this reason, the theoretical results are not displayed in Fig. 1 at angles less than 30°.

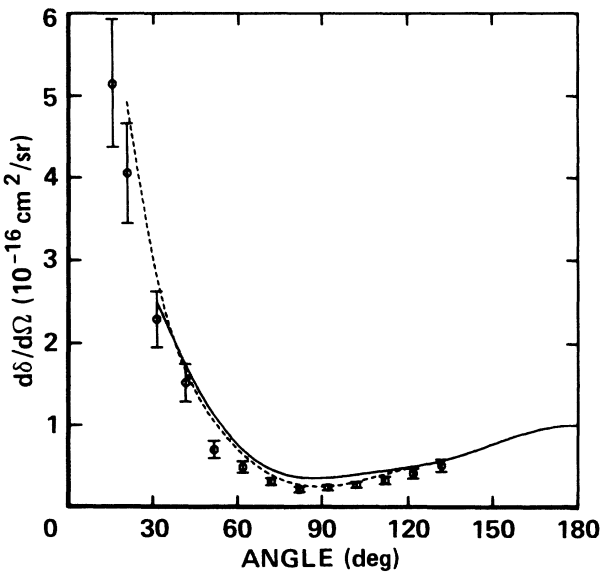

FIG. 1. Elastic differential cross sections in units of 10^{-16} cm^2/sr at 20 eV. Present theory, basis set A (——); experiment from Ref. 44 (○○○); experiment from Ref. 45 (— — —).

We see from Table II that the elastic integral cross section at 15 eV is in good agreement with the experiment of Tanaka, Srivastava, and Chutjian,[44] but at 20 eV we find an 11% difference. Table II also presents the elastic cross sections at 9.9 and 10.3 eV, just below the inelastic threshold, with the $b\,^3\Sigma^+$ channel included as a closed channel. Comparison is made with the elastic cross sections of Tanaka, Srivastava, and Chutjian[44] at 9.9 eV. Our results are considerably larger in magnitude. This is consistent with other theoretical calculations[3] in this energy region. A possible cause could be the neglect of polarization and an overestimation of the flux going into the elastic channel when the inelastic open channels and dissociative attachment channels are not explicitly included in the calculations.

In the following discussion of the inelastic transition, we will present data that are consistent with the picture that the open-channel threshold structure of the cross section is dominated by the decay of the $(5\sigma)(3s\sigma)^2{:}^2\Sigma^+$ state of CO^- into various partial waves. The discussion

TABLE II. Elastic cross section, theory and experiment (see Ref. 40), and inelastic cross section, for $X\,^1\Sigma^+ \rightarrow b\,^3\Sigma^+$, theory. Cross sections are in a_0^2.

Energy (eV)	Present theory elastic	Experiment elastic	Present theory inelastic
9.90	52.64	45.60	
10.30	51.37		
10.66	53.43		0.089
10.68	53.27		0.249
10.70	53.13		0.319
10.80	52.54		0.423
10.85	52.29		0.467
10.90	52.05		0.405
11.00	51.54		0.263
11.10	51.02		0.254
11.20	50.53		0.298
11.30	50.07		0.348
11.50	49.28		0.404
11.70	48.53		0.410
12.00	47.48		0.315
12.50	45.98		0.218
13.00	44.65		0.258
13.40	43.75		0.266
14.00	42.59		0.254
15.00	41.01	39.64	0.283
16.00	39.88		0.305
16.50	39.45		0.301
18.00	38.57		0.262
20.00	38.26	33.93	0.242

is facilitated by the presentation of integral and differential cross sections as well as graphs of resonant K-matrix elements and resonant partial-wave eigenphases.

We begin with Fig. 2, which presents the integrated cross section for the inelastic transition $X\,^1\Sigma^+ \rightarrow b\,^3\Sigma^+$. In addition to the results calculated using basis set A (solid curve), we also present cross sections using a second basis set, set B (dashed curve). This set is obtained by deleting the d functions in set A. The integrated cross sections calculated with set A are also presented in Table II. The cross sections from the two sets (A and B) of calculations are similar, except for the fact that the peak heights are reversed. The insertion errors are significantly reduced by the inclusion of the d functions (set A) as compared with the s and p basis set (set B). The difference between the α-insertion and k-insertion results (set A) is approximately 10% at 10.85 eV, indicating an acceptable level of convergence in the VGV [see Eq. (9)] term. Thus we conclude that our inelastic cross sections are adequately converged with respect to basis set size. The first peak at 10.87 eV is the narrowest. A lower and broader peak occurs at 11.6 eV. A third peak is located at about 13.4 eV, and a broader but larger peak at approximately 16.2 eV is also shown in Fig. 2.

In order to understand the physical origin of the four local maxima observed in the inelastic cross section, a partial-wave analysis was performed. To aid in this analysis, we present in Table III the contribution of the $^2\Sigma$ and $^2\Pi$ symmetries to the inelastic cross section as a

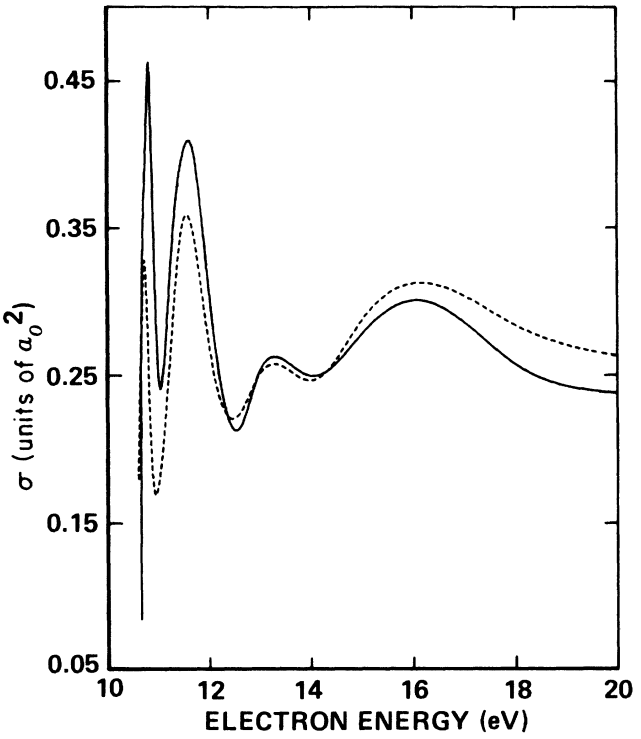

FIG. 2. Inelastic integrated cross sections in units of a_0^2/sr for $X\,^1\Sigma^+ \rightarrow b\,^3\Sigma^+$. Present theory, k insertion; basis set A (——); basis set B (— — —).

TABLE III. Contributions of the $^2\Sigma$ and $^2\Pi$ symmetries to the inelastic cross section for the $X\,^1\Sigma^+ \rightarrow b\,^3\Sigma^+$ transition, and to the excited elastic cross section $b\,^3\Sigma^+ \rightarrow b\,^3\Sigma^+$. Cross sections are in a_0^2. The energies are in electron volts (eV).

Energy (eV)	$^2\Sigma$ Inelastic cross section	$^2\Pi$ Inelastic cross section	$^2\Sigma$ $b\,^3\Sigma^+$ elastic cross section	$^2\Pi$ $b\,^3\Sigma^+$ elastic cross section
10.66	0.089	0.000	2.655(3)	2.042(1)
10.68	0.248	0.000	3.583(3)	3.198(2)
10.70	0.318	0.001	3.031(3)	1.655(3)
10.80	0.420	0.003	1.217(3)	1.114(3)
10.85	0.464	0.004	8.870(2)	8.368(2)
10.90	0.401	0.005	7.277(2)	6.815(2)
11.00	0.258	0.006	6.206(2)	5.129(2)
11.10	0.248	0.007	6.976(2)	4.255(2)
11.20	0.290	0.008	6.828(2)	3.732(2)
11.30	0.338	0.009	5.707(2)	3.368(2)
11.50	0.391	0.013	3.330(2)	2.771(2)
11.70	0.393	0.017	2.109(2)	2.234(2)
12.00	0.290	0.025	1.117(2)	1.682(2)
12.50	0.182	0.036	6.666(1)	1.177(2)
13.00	0.215	0.043	5.687(1)	8.781(1)
13.40	0.220	0.046	5.161(1)	7.242(1)
14.00	0.206	0.049	4.954(1)	6.263(1)
15.00	0.234	0.048	5.786(1)	2.149(1)
16.00	0.260	0.045	6.216(1)	8.946
16.50	0.259	0.043	6.224(1)	8.512
18.00	0.221	0.041	6.196(1)	7.817
20.00	0.188	0.054	5.313(1)	8.076

function of energy. The dominance of the $^2\Sigma$ symmetry is clearly demonstrated. We also present in Table III the elastic cross section for the excited b state, decomposed by symmetry. The large peak in the excited elastic cross section in the $^2\Pi$ symmetry at about 10.7 eV is very obvious. No corresponding $^2\Pi$ peak is found in the inelastic cross section and the structure and the excited-state elastic $^2\Pi$ channel does not seem to influence our results for the inelastic cross section in a significant way.

It should be noted that the projectile angular momentum quantum number l is not conserved for the case or a nonspherical potential. Thus the analysis of the resonance behavior in electron-molecule scattering is more complicated than for electron-atom scattering. In addition, we are considering an inelastic process. The eigenphase sum analysis[46] that is so useful for elastic electron-atom scattering is not so clearly and unambiguously defined in the present case. The eigenphase sum is defined according to the symmetries of the scattering system, which are $^2\Sigma$ and $^2\Pi$ in the present case. We considered the l's 0,1,2. The departure of the present analysis from that described in Ref. 46 is that, for a given process and a given symmetry, we include the possibility that the resonance behavior may occur in different partial waves and at different energies. Our analysis also applies to the case of overlapping resonances. As a result, we calculate partial resonance positions and widths for each process. However, the inelastic process of present interest is unavoidably connected with the elastic processes when the S-matrix diagonalization is performed to construct the partial eigenphases. Thus it is not considered illuminating to construct resonance positions and widths as is done in Ref. 46.

In order to gain additional insight into the nature of the peak structure, a bound state (SCF plus IVO) calculation of the energy of the $^2\Sigma^+$ state of CO^- was done using the $(5\sigma)(3s\sigma)^2$ configuration. The resulting energy was 11.044 eV, approximately 1 eV above the experimental value of 10.04 eV,[28] and lies above the $b\ ^3\Sigma^+$ threshold energy. This computed energy indicates that the CO^+ state (5σ:$^2\Sigma^+$), the grandparent state,[28] must be well correlated in order to accommodate the two Rydberg electrons. Only then can one expect the CO^- energy to agree with experiment. Since the present SMC calculation uses a frozen-core representation, we should expect the CO^- resonances in $^2\Sigma^+$ system symmetry to be higher in energy than experiment. Thus the resonance appears as an open-channel core-excited shape resonance in the theoretical calculations, while in experiment, it appears as a close-channel Feshbach resonance in the elastic channel. As seen from Table II, we did not find a Feshbach resonance below the $b\ ^3\Sigma^+$ threshold, only a slight dip in the elastic cross section associated with opening up the inelastic channel. An analysis of the elastic K-matrix elements and the corresponding partial eigenphases also fail to indicate a resonance immediately below threshold.

The difficulty of calculating an accurate energy for negative ions is known.[47–49] In the case of the oxygen atom, Sasaki and Yoshimine[47] obtained an electron affinity of 1.041 eV using a singles and doubles configuration interaction (SDCI) treatment, 0.421 eV smaller than the experimental value[50] at 1.462 eV. A more sophisticated calculation of Bauschlicher *et al.*,[49] which is done at the full configuration interaction CI level of correlation, obtains an electron affinity of the oxygen atom to be 1.290 eV, which differs from experiment by 0.172 eV. These calculations show that a highly correlated wave function is required to describe the negative ion. It is not surprising that the present calculation, using uncorrelated target functions and neglecting e-target correlation except at a two-state level, results in an error of 1.0024 eV in the position of the resonance.

We have investigated the possibility of artificially producing a Feshbach resonance below the excitation threshold by shifting the energy position of the neutral CO $b\ ^3\Sigma^+$ target state with respect to the negative-ion state. Since the experimental Feshbach resonance energy position[28] (10.04 eV) is approximately 0.36 eV below the experimental threshold energy position[41] (10.40 eV), we have shifted the theoretical threshold to 11.404 eV, which is 0.36 eV above the bound-state (SCF plus IVO) energy (11.044 eV) calculated for the $^2\Sigma^+$ state of CO^-. We have done a thorough scan below threshold and have been unable to detect a resonance structure. In addition, the basic integral cross-section structures above threshold did not change except a shift to a higher energy corresponding to the 0.36-eV threshold shift. This result is consistent with the discussion in the preceding paragraph that the error in the position of the resonance is due to insufficient correlation. For our final result, we chose to use a purely *ab initio* set of scattering parameters because the intent of our study is to judge the reliability of purely *ab initio* calculations without recourse to empirical adjustments based on experiment.

The two lowest energy peaks are too close together in energy to be considered isolated. The width of the 11.6-eV peak is sufficently large so as to overlap the 10.87-eV resonance. The two higher energy peaks are broad and weak and are also not isolated. The possible resonance behavior is analyzed by considering the behavior of the K-matrix elements and of the partial eigenphases. This is done for the inelastic matrix elements as well as the excited-state elastic matrix elements and for the partial-wave eigenphases. Both inelastic and excited-state elastic quantities exhibit resonance behaviors, but generally at somewhat different energies. The $^2\Sigma^+$ core excited resonance can also manifest itself in the ground-state elastic channel. However, our analysis of the ground-state elastic K-matrix elements and eigenphases failed to find any resonance behavior. Since the coupling between the negative ion $(5\sigma)(3s\sigma)^2$ and the elastic channel $(5\sigma)^2(k\sigma)$ is a correlation effect, it is possible that the present two-state approximation is not sufficiently correlated to account for the experimental Feshbach resonance in the elastic channel.

It has also been pointed out[21] that in the vicinity of a resonance, the completeness requirement for the insertion calculation of the VGV term is severely tested. Although the validity of the cross-section calculation can be tested by comparing the α insertion and the k insertion, the validity of the behavior of the K-matrix elements and partial eigenphases as a function of scattering energy is more

difficult to judge. In fact, a large insertion basis is required to produce the exactly correct behavior at energies very near the resonance energy.[21] This is true, even though the cross sections are not nearly as sensitive to the exact convergence of the VGV insertion basis. Nevertheless, a thoughtful consideration of the K-matrix elements and partial eigenphases can, even when more than one open channel is present, give substantial insight into the nature of the resonance behavior.

We present, in Table IV, selected inelastic K-matrix elements at the energies near the four-peak positions, for the dominant $^2\Sigma$ symmetry. The dominant partial-wave contribution at 11.7, 13.4, and 16.0 eV comes from s waves in both the incident and the exit channel. At 10.85 eV, the dominant contribution is from an incident s wave and an exit $p\sigma$ wave. At 11.7 eV, the second most important contribution comes from an incident $d\sigma$ wave and an exit s wave. There is also a significant contribution from an incident $p\sigma$ wave and an exit s wave. At 13.4 eV, incident $p\sigma$ and $d\sigma$ waves with outgoing s waves are of almost equal magnitude as the second most dominant contribution after the incident and exit s waves. For the peak at approximately 16.2 eV, the tabulated K-matrix elements in Table IV show no clear partial- wave dominance.

Specific evidence for resonance behavior can be seen most clearly by examining the K-matrix elements. Further evidence is obtained from the partial eigenphases. We begin with the inelastic K-matrix elements. The inelastic $^2\Sigma^+$ K-matrix elements considered (l:0,1,2) all showed the discontinuous behavior characteristic of a pole between 10.9 and 11.5 eV except for those partial waves with an exit $d\sigma$ wave. We show this behavior for selected partial waves in Fig. 3. We also note that this is the only energy region where the inelastic K-matrix elements showed discontinuous behavior. There is no evidence of discontinuous K-matrix behavior in the $^2\Pi$ symmetry for the inelastic excitation process.

We next consider the elastic K-matrix elements for the excited state. We show in Figs. 4(a) and 4(b) the discontinuities in the s wave in and s wave out, $^2\Sigma^+$ K-matrix elements. There are also discontinuities for $p\sigma$ waves and $d\sigma$ waves in the vicinity of the 16.5 eV peak for $^2\Sigma^+$

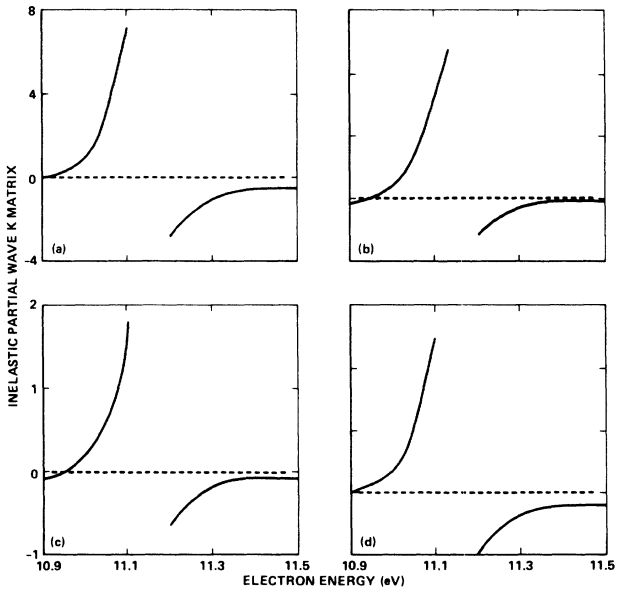

FIG. 3. Selected resonant $^2\Sigma^+$ inelastic K-matrix elements labeled by $l_i \rightarrow l_f$. (a) $0\rightarrow 0$, (b) $0\rightarrow 1$; (c) $1\rightarrow 1$; (d) $2\rightarrow 0$.

symmetry. Figures 4(c) and 4(d) shows the $p\pi$-wave K-matrix discontinuities for the $^2\Pi$ system symmetry. There is also a discontinuity in the $d\pi$ wave for $^2\Pi$ symmetry in the vicinity of the 11.6-eV peak. It should be noted in Fig. 4 that the discontinuities in Figs. 4(a) and 4(d) show a qualitatively different energy dependence than in Figs. 4(b) and 4(c). It is known that at a resonance, the partial eigenphase shift δ_l sharply increases by $(\pi/2)(\mathrm{mod}\pi)$.[51] This then implies that the K-matrix discontinuity must increase on the low-energy side and decrease on the high-energy side as in Figs. 4(b) and 4(c). The behavior in Figs. 4(a) and 4(d) is consistent with a partial eigenphase shift that decreases through $(\pi/2)(\mathrm{mod}\pi)$. Newton[51] described this type of collision as a "time advance." It should be further pointed out that the sign of the off-diagonal K-matrix elements is ar-

TABLE IV. Selected ($^2\Sigma$) K-matrix elements for the inelastic $X\,^1\Sigma^+ \rightarrow b\,^3\Sigma^+$ transition at four energies near the resonance positions.

Entrance channel (l,m)	Exit channel (l,m)	K-matrix elements 10.85 eV	11.70 eV	13.40 eV	16.00 eV
(0,0)	(0,0)	0.15	0.52	0.37	0.18
(0,0)	(1,0)	0.30	0.15	0.16	0.13
(0,0)	(2,0)	0.04	0.05	0.10	0.14
(1,0)	(0,0)	0.06	0.29	0.26	0.15
(1,0)	(1,0)	0.16	0.10	0.13	0.09
(1,0)	(2,0)	0.02	0.03	0.07	0.10
(2,0)	(0,0)	0.07	0.35	0.27	0.15
(2,0)	(1,0)	0.18	0.13	0.13	0.13
(2,0)	(2,0)	0.03	0.04	0.09	0.13

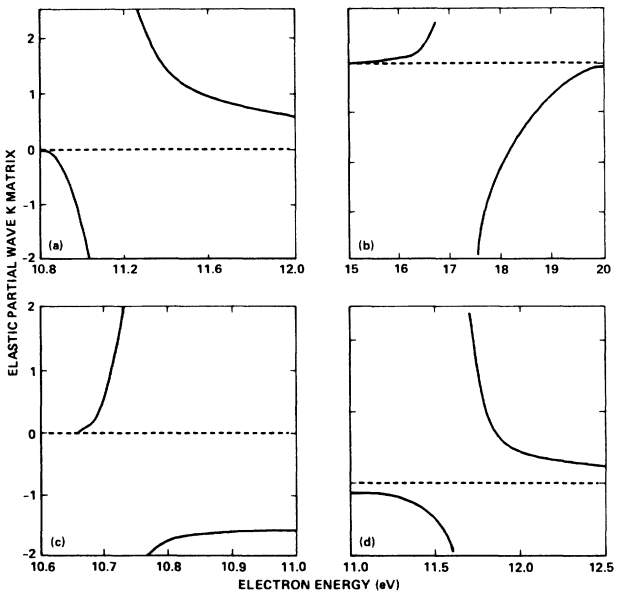

FIG. 4. Selected resonant $^2\Sigma^+$ and $^2\Pi$ excited elastic K-matrix elements labeled by $l_i \rightarrow l_f$. (a) $^2\Sigma^+$:0→0, (b) $^2\Sigma^+$:0→0; (c) $^2\Pi$:1→1; (d) $^2\Pi$:1→1.

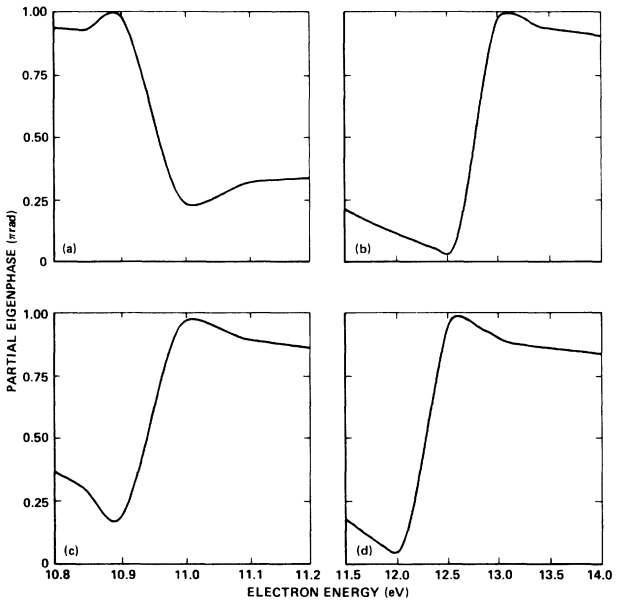

FIG. 5. Selected resonant $^2\Sigma^+$ excited elastic partial eigenphases labeled by the channel component number [component 1 corresponds to active target electron spin assignment $(\alpha\beta+\beta\alpha)_t$ and component 2 to $(\alpha\alpha)_t$ or $(\beta\beta)_t$] and labeled by $l_i \rightarrow l_f$ in units of π. (a) Excited elastic component 1 (0→0), (b) excited elastic component 1 (0→0), (c) excited elastic component 2 (0→0), (d) excited elastic component 2 (0→0).

bitrary, but the sign of the diagonal elements is not, so that this contrasting energy dependence in the excited elastic K-matrix elements is not arbitrary with respect to the sign.

The term time advance is used generically by Newton[51] to indicate a sharply decreasing phase shift as opposed to "time delay," which means a sharply increasing phase shift. Only in the case of time delay is the increase through $\pi/2$ radians over a narrow energy range. Then the label resonance be used to describe this phase shift behavior. However, the term "narrow energy range" is left somewhat imprecisely defined. If the rapid energy variation occurs in a particular partial wave over an energy region where the other phase shifts are changing slowly, then they play the part of the resonance background and the definition of narrow energy region is easily given in each particular case. If, on the other hand, the other partial waves have rapidly decreasing phase shifts over the energy region where the supposed resonance is undergoing a rapid increase in phase shift, then interference effects can occur and obscure the resonance signature. Thus, a time advance could result from a predominantly repulsive effect for the rapidly changing phase shift, or it could result from the interference effect of a strong nonresonant background scattering.[52–54] At our present level of understanding of these phenomena, it is not clear how to distinguish these various possibilities. Thus we shall use the term time advance to indicate a rapidly changing phase shift, which decreases through $\pi/2$ radians over a narrow energy region, with the unavoidable imprecision in the definition of the width of the aforementioned energy region.

In Figs. 5(a)–5(d), the excited elastic, s-wave eigenphases corresponding to one of the two degenerate components of the excited-state elastic channel are presented for the $^2\Sigma^+$ symmetry for two resonance energy regions. The two components of the excited elastic channel are classified according to the spin assignments of the two active electrons of the target. Component 1 corresponds to the $S_z=0$ symmetric combination $(\alpha\beta+\beta\alpha)_t$. Component 2 corresponds to $S_z=\pm 1$, which results in $(\alpha\alpha)_t$ or $(\beta\beta)_t$. Figure 5(a) shows the signature of time-advance scattering as mentioned above. This partial eigenphase is associated with the K-matrix discontinuity shown in Fig. 4(a). It should be pointed out that the resonance structures of Figs. 4(b) and 5(b) are different as can be seen by the energy ranges. The width and resonance energy corresponding to the three resonance parts of Fig. 5 are presented in Table V. The resonance of Fig. 5(c) is associated with the 10.87-eV peak and the resonances of Figs. 5(b) and 5(d) are associated with the 11.6-eV peak.

Now considering the 13.4-eV peak, no discontinuous K-matrix behavior is evident in either of the inelastic $^2\Sigma$ or $^2\Pi$ symmetries. There are sign changes in the excited elastic K-matrix elements for both symmetries in the vicinity of the 13.4-eV peak, but no evidence for discontinuous behavior. Neither is there any clear evidence of resonance behavior in the partial eigenphases of either symmetry. Thus the origin of this peak is not clear.

We finally consider the peak at 16.2 eV. There is no evidence for discontinuous inelastic K-matrix behavior in the vicinity of this peak for either the $^2\Sigma$ or $^2\Pi$ symmetry. However, the $^2\Sigma$ symmetry for the excited elastic process

TABLE V. Resonance [Figs. 5(b)–5(d)] energies and widths in $^2\Sigma$ symmetry for the excited-state elastic channel.

	Fig. 5(b) component 1	Fig. 5(c) component 2	Fig. 5(d) component 2
Energy (eV)	12.74	10.95	12.22
Γ (meV)	49.0	6.6	57.0

exhibits discontinuous K-matrix elements for s waves, $p\sigma$ waves, and $d\sigma$ waves. The $p\sigma$ waves give the weakest discontinuity while the s and $d\sigma$ waves have about the same strength of discontinuity. The $^2\Pi$ symmetry has no evidence of K-matrix discontinuity near the 16.2-eV peak, for the excited elastic process.

The 10.87 and 11.6 eV peaks are two of the most interesting results from the present calculation. Partial-wave analysis shows that these peaks come from the $^2\Sigma$ partial channel. This is to be contrasted with the $^2\Pi$ resonance in the elastic scattering of the ground state at about 2.0 eV. Although the inelastic peak does not appear to be as sharp and long lived as the vibrational peaks common in polar molecules right above vibrational thresholds,[2,3] there are similarities. In the exit channel the electron has lost most of its kinetic energy to the molecular target and is moving slowly in the presence of the enhanced dipole field of the excited molecule, which is attractive and tends to further delay the electron, resulting in the formation of a temporary negative ion.

In Figs. 6(a)–6(d) the integrated inelastic cross sections calculated with basis set A are compared with available experimental data from threshold to 14 eV. Figure 6(a) is the present theory result. Figure 6(b) is the experimental data of Allan[33] and Fig. 6(c) is the optical experimental data from Ref. 29. Figure 6(d) shows the experimental results of Newman, Zubek, and King.[30] The disagreement in magnitude among the various results is apparent. However, all results show one or two low-energy peaks.

The experiment of Allan employed a trochoidal electron spectrometer that is especially sensitive to processes with small cross sections.[33] The measured cross section is a superposition of differential cross sections at 0° and 180° and thus the shape may differ from the true integral cross section if the angular distributions vary with energy. Nevertheless, Allan's data show a sharp peak just above the threshold, in qualitative agreement with our present result. Also, there are four structures, albeit of much different sizes than ours, in Allan's data.

Skubenich's cross section in Fig. 6(c) is the only experiment that has units associated with the cross section and is almost an order of magnitude smaller than our two-channel cross sections. Recent multichannel calculations[55,56] on the valence excitations of N_2 showed that unitarized two-state calculations tend to overestimate the excitation cross sections because available open channels responsible for the loss of the incident flux are not properly accounted for. On the other hand, the electron-

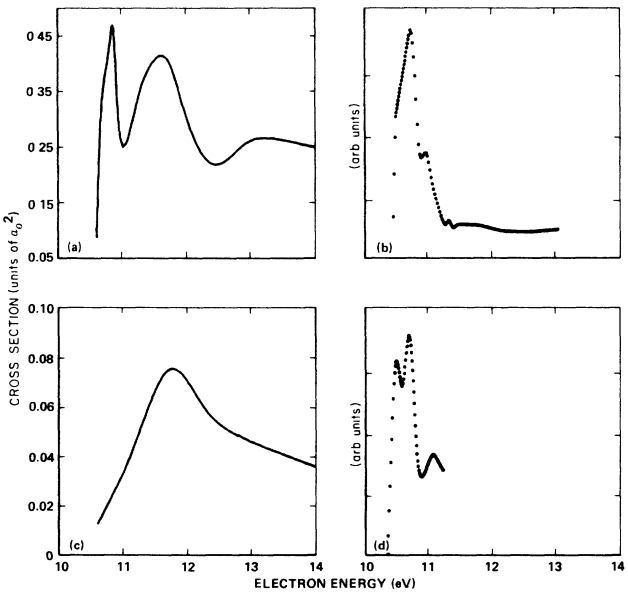

FIG. 6. Inelastic integrated cross sections in units of a_0^2 for $X\,^1\Sigma^+ \rightarrow b\,^3\Sigma^+$. (a) Present theory, (b) experiment from Ref. 33, (c) experiment from Ref. 29, (d) experiment from Ref. 30.

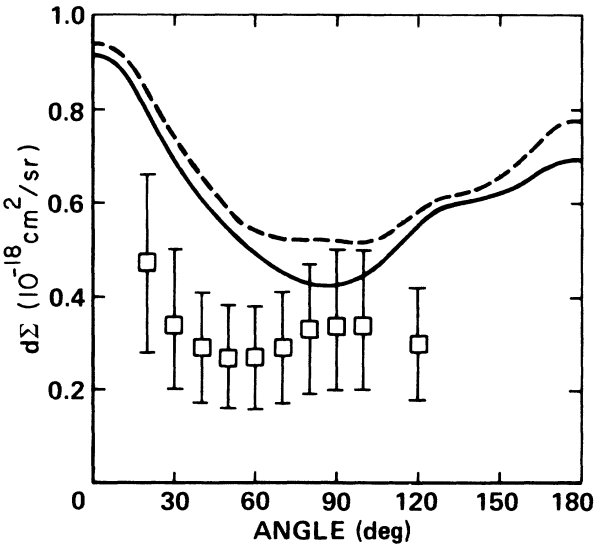

FIG. 7. Inelastic differential cross sections in units of 10^{-18} cm^2/sr for $X\,^1\Sigma^+ \rightarrow b\,^3\Sigma^+$. Present theory at 20 eV, basis set A (——), basis set B (— — —), experiment from Ref. 32 (□□□).

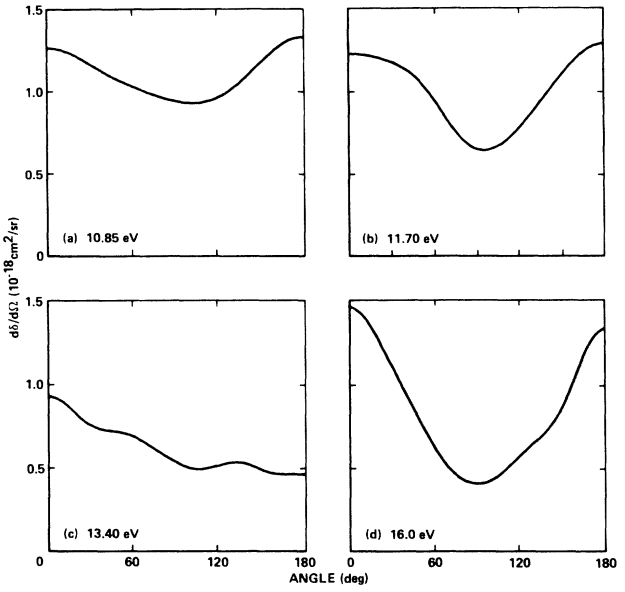

FIG. 8. Inelastic differential cross sections in units of 10^{-18} cm^2/sr for $X\,^1\Sigma^+ \rightarrow b\,^3\Sigma^+$. Present theory, basis set A; graph (a), 10.85 eV; graph (b), 11.70 eV; graph (c), 13.40 eV; graph (d), 16.00 eV.

impact excitation cross sections for the $X\,^1\Sigma_g^+ \rightarrow b\,^3\Sigma_u^+$ state of H_2 calculated in the two-state approximation[8-11] are in good agreement with experiment. We note that the N_2 states studied by Huo and co-worker[55,56] are valence excited states, whereas the $X \rightarrow b$ transition of H_2, like the transition in the present study, is a Rydberg transition. Whether the nature of the excitation plays an important role in determining the amount of channel coupling remains to be studied.

Figure 7 presents our inelastic differential cross section at 20 eV obtained with basis set A (solid curve), basis set B (dashed curve), and the experimental differential cross section of Trajmar, Williams, and Cartwright[32] (squares with error bars). The agreement between basis set A and B is good, both in shape and magnitude. The agreement with the data of Trajmar, Williams, and Cartwright is only qualitative. Both theory and experiment show forward peaking and a broad minimum. The calculated minimum is near 90° whereas the experimental minimum is close to 60°. While our calculation shows a distinct backward peaking, experiment did not extend to large enough angles to confirm this. It is interesting to note that if we extrapolate the differential cross section of Trajmar, Williams, and Cartwright and integrate over angles, an integral cross section will be obtained that is approximately two to three times smaller than theory, and hence significantly larger than the optical data of Skubenich.[29] It should also be pointed out that Zetner and Trajmar[7] showed recently the differential cross-section measurements reported in Ref. 32 may be subject to large uncertainties due to problems with stray electrons and overlapping bands. In view of the experimental difficulties, no firm conclusion can be drawn from the comparison.

Because each resonance results from a mixture of partial waves, the nature of the resonances is not clearly indicated by the shape of the differential cross-section curves. In this respect, our results indicate that the common practice of relying on the shape of the differential cross section to deduce the symmetry of the negative-ion resonance may be questionable, at least for some transitions. For these same reasons, it is more informative to look at partial eigenphases and K-matrix elements rather

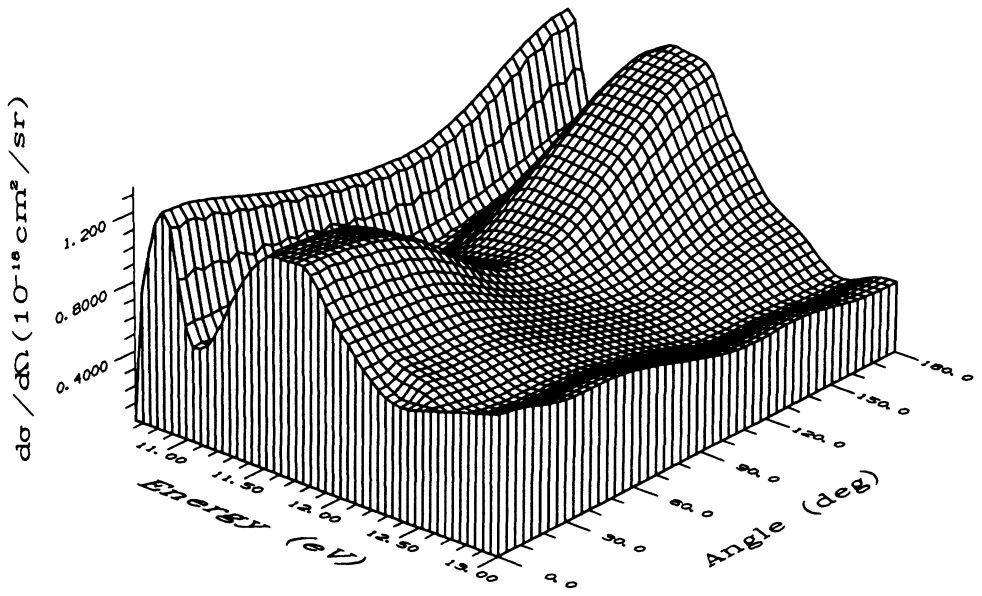

FIG. 9. Energy vs angle surface fit of the inelastic differential cross section in units of 10^{-18} cm^2/sr for $X\,^1\Sigma^+ \rightarrow b\,^3\Sigma^+$.

than eigenphase sums, in order to analyze resonance behavior.

Figure 8 presents the inelastic differential cross sections at 10.85, 11.70, 13.40, and 16.00 eV. The curve at 10.85 eV is rather flat and somewhat asymmetrical indicating an admixture of s and $p\sigma$ waves. The curves at 11.70 and 16.00 eV have deep minima. This is probably a reflection of the importance of $d\sigma$-wave $\rightarrow s$-wave scattering (see Table IV). The curve at 13.40 eV shows a decline from low to high angles with various small wiggles, probably indicating interference effects.

Finally, in Fig. 9, we present a plot of a surface fit of the inelastic differential cross section from 10.60 to 13.00 eV. In the vicinity of the two resonances located in this energy interval, the differential cross-section (DCS) peaks both in the forward and backward direction and a local minimum is found near 90°. The DCS surface shows a deep trench immediately after each resonance peak. In the nonresonant region near 13 eV, the DCS curve is relatively flat and shows no backward peak.

IV. CONCLUSIONS

The $X\,^1\Sigma \rightarrow b\,^3\Sigma^+$ transition of CO has been described using the Schwinger multichannel method in the two-state approximation, in an energy range from threshold to 20 eV. Four peaks in the inelastic cross section were found at approximately 10.87, 11.6, 13.4, and 16.2 eV. All except the 13.4-eV peak were identified as resonance structures. From an analysis of the K matrices and the partial eigenphases, it was also determined that time advance scattering behavior contributes to the 10.87-eV peak. The $^2\Sigma^+$ symmetry was found to dominate the cross section at this level of the target-state coupling. As more states are coupled, the extent of this dominance could be modified. The compound state of CO^- of $^2\Sigma^+$ symmetry was found to control the inelastic process just above threshold resulting in the 10.87 and 11.6-eV peaks. These seem to be structures that result from decay of the configurations $(5\sigma)(3s\sigma)^2\,^2\Sigma^+$ and $(5\sigma)(3s\sigma)(3p\sigma):^2\Sigma^+$ into the inelastic channel. The 10.87-eV peak seems to be predominantly $5\sigma 3s\sigma 3p\sigma$ with an admixture of $5\sigma 3s\sigma^2$ while the 11.6-eV peak is apparently predominantly $5\sigma 3s\sigma^2$ with an admixture of $5\sigma 3s\sigma 3p\sigma$.

An SCF calculation of the energy of the $^2\Sigma^+$ CO^- state with a frozen core resulted in an energy of 11.044 eV. Experimentally, this state is identified with a core-excited Feshbach resonance at 10.04 eV, below the $b\,^3\Sigma^+$ threshold. Thus the present SMC calculation, apparently due to insufficient correlation, places the closed-channel 10.04-eV Feshbach resonance as an open-channel shape resonance. Experimentally, the large width of this Feshbach resonance (approximately 45 meV) produces a sharp open-channel threshold structure as a result of the decay in the wings of this resonance, into the open channel. We see this effect as a direct decay into the open channels.

The small peak at 13.4 eV is not identifiable as a resonance, but rather appears to be an interference effect among the various partial waves. The 16.2-eV peaks appears to be a shape resonance, also in the $^2\Sigma^+$ symmetry. It is possibly associated with the compound CO^- state; however, the energy separation from the SCF energy of 11.044 eV for this state argues against this association. The resonance appears to be limited to the excited-state elastic channel. No resonance indications were observed in the inelastic K-matrix elements.

This study clearly shows that present day *ab initio* theories are capable of describing resonances in electron-molecule inelastic collisions. To understand these processes, a systematic and detailed investigation must be conducted, beginning at the two-state level. The extension of the present study explicitly including additional channels is underway. We might also state that two-state calculations on an analogous transition $X\,^1\Sigma_g^+ \rightarrow E\,^3\Sigma_g^+$ of N_2 also showed core-excited Rydberg resonances.[37] These results, along with other work on N_2, clearly indicate that resonances play an important role in low-energy electron-molecule inelastic scattering.

ACKNOWLEDGMENTS

The research of C.A.W. is supported by the National Science Foundation Grant No. PHY-8711805 and NASA Ames Cooperative Agreement No. NCC 2-492. The help and advice of the staff at the NASA Ames Central Computing Facility in using the CRAY XMP-48 and the Numerical Aerodynamic Simulation Facility, at NASA Ames, in using the CRAY 2, is acknowledged. C.A.W. would also like to acknowledge a grant of computer time from the Florida State University Supercomputer Computations Research Institute.

[1] *Electron-Atom and Electron-Molecule Collisions,* edited by J. Hinze (Plenum, New York, 1983), and references therein.

[2] S. Trajmar, D. F. Register, and A. Chutjian, Phys. Rep. **97**, 219 (1983), and references therein.

[3] G. Csanak, D. C. Cartwright, S. K. Srivastava, and S. Trajmar, in *Electron-Molecule Interactions and Their Applications,* edited by L. G. Christophorou (Academic, Orlando, 1984), p. 1, and references therein.

[4] S. Trajmar and D. C. Cartwright, in Ref. 3, p. 156, and references therein.

[5] C. S. Willet, in *Introduction to Gas Lasers: Population Inversion Mechanisms* (Pergamon, New York, 1974).

[6] Ph. Avouris and J. E. Demuth, Ann. Rev. Phys. Chem. **34**, 49 (1984).

[7] P. W. Zetner and S. Trajmar, in *Abstracts of the Fifteenth Interantional Conference on the Physics of Electronic and Atomic Collisions,* edited by J. Geddes, H. B. Gilbody, A. E. Kingston, C. J. Latimer, and H. J. R. Walters (Queen's University, Belfast, 1987).

[8] B. I. Schneider and L. A. Collins, J. Phys. B **18**, L857 (1985).

[9] K. L. Baluja, C. J. Noble, and J. Tennyson, J. Phys. B **18**, L851 (1985).

[10] M. A. P. Lima, T. L. Gibson, and W. M. Huo, and V. McKoy, J. Phys. B **18**, L865 (1985).

[11] B. I. Schneider and T. N. Rescigno, Phys. Rev. A **37**, 3749 (1988).

[12]K. Takatuska and V. McKoy, Phys. Rev. A **24**, 2473 (1981).
[13]K. Takatuska and V. McKoy, Phys. Rev. A **30**, 1734 (1984).
[14]T. L. Gibson, M. A. P. Lima, K. Takatsuka, and V. McKoy, Phys. Rev. A **30**, 3005 (1984).
[15]M. A. P. Lima, T. L. Gibson, V. M. Huo, and V. McKoy, Phys. Rev. A **32**, 2696 (1985).
[16]L. M. Brescansin, M. A. P. Lima, T. L. Gibson, V. McKoy, and W. M. Huo, J. Chem. Phys. **85**, 1854 (1986).
[17]M. A. P. Lima, T. L. Gibson, K. Takatuska, and V. McKoy, Phys. Rev. A **30**, 1741 (1984).
[18]S. Nagano, Z.-P. Luo, H. Metiu, W. M. Huo, M. A. P. Lima, and V. McKoy, J. Chem. Phys. **85**, 6153 (1986).
[19]S. Chung and C. C. Lin, Phys. Rev. A **17**, 1874 (1978).
[20]C. A. Weatherford, Phys. Rev. A **22**, 2519 (1980).
[21]W. M. Huo, T. L. Gibson, M. A. P. Lima, and V. McKoy, Phys. Rev. A **36**, 1632 (1987).
[22]W. M. Huo, M. A. P. Lima, T. L. Gibson, and V. McKoy, Phys. Rev. A **36**, 1642 (1987).
[23]J. E. Land, J. Appl. Phys. **49**, 5716 (1978).
[24]G. D. Billing, Chem. Phys. **86**, 349 (1984).
[25]M. H. Tsai, T. N. Rhodin, R. Kasowski, J. Vac. Sci. Technol. A **2**, 1016 (1984).
[26]S. Saha, S. Ray, B. Bhattacharyya, and A. K. Barua, Phys. Rev. A **23**, 2926 (1981).
[27]G. P. Menees, J. Spacecr. Rockets **22**, 37 (1985); D. M. Cooper, R. L. Jaffee, and J. O. Arnold, *ibid.* **22**, 60 (1985).
[28]G. J. Schulz, Rev. Mod. Phys. **45**, 423 (1973).
[29]V. V. Skubenich, Opt. Spectrosc. **23**, 540 (1967).
[30]D. S. Newman, M. Zubek, and G. C. King, J. Phys. B **16**, 2247 (1983), and references therein.
[31]J. P. Polley and T. L. Bailey, Phys. Rev. A **37**, 733 (1988).
[32]S. Trajmar, W. Williams, and D. C. Cartwright, in *Abstracts of the Eighth International Conference on the Physics of Electronic and Atomic Collisions, Belgrade, 1973,* edited by B. C. Cŏblić and M. V. Kurepa (Grafičko Preduzeće "Budućnost", Zrenjanin, 1973), p. 349.
[33]M. Allan (private communication).
[34]T. Sawada, D. L. Sellin, and A. E. S. Green, J. Geophys. Res. **77**, 4819 (1972).
[35]S. Chung and C. C. Lin, Phys. Rev. A **9**, 1954 (1974).
[36]H. Feshbach, Ann. Phys. (N.Y.) **19**, 287 (1962).
[37]N. F. Lane, Rev. Mod. Phys. **52**, 29 (1980).
[38]M. A. P. Lima, T. L. Gibson, V. McKoy, and W. M. Huo, Phys. Rev. A **38**, 4527 (1988).
[39]W. J. Hunt and W. A. Goddard, Chem. Phys. Lett. **3**, 414 (1969).
[40]S. Huzinaga, J. Chem. Phys. **42**, 1293 (1965).
[41]B. J. Ransil, Rev. Mod. Phys. **32**, 239 (1960).
[42]A. Szabo and N. S. Ostlund, *Modern Quantum Chemistry* (Macmillan, New York, 1983).
[43]The AMES SMC was written by Huo, Gibson, and Lima. An earlier code based on the present method was written by Takatsuka, Gibson, Lima, and McKoy (see Ref. 17).
[44]J. Tanaka, S. K. Srivastava, and A. Chutjian, J. Chem. Phys. **69**, 5329 (1978).
[45]J. C. Nickel, C. Mott, I. Kanik, and D. C. McCollum (unpublished).
[46]A. U. Hazi, Phys. Rev. A **19**, 920 (1979), and references therein.
[47]F. Sasaki and Y. Yoshimine, Phys. Rev. A **9**, 26 (1974).
[48]J. Comer and F. H. Read, J. Phys. B **4**, 1678 (1971).
[49]C. W. Bauschlicher, Jr., S. R. Langhoff, H. Partridge, and P. R. Taylor, J. Chem. Phys. **85**, 3407 (1986).
[50]H. Hotop and W. C. Lineberger, J. Chem. Ref. Data **4**, 539 (1975).
[51]R. G. Newton, *Scattering Theory of Waves and Particles,* 2nd ed. (Springer-Verlag, New York, 1982).
[52]G. C. Schatz and A. Kuppermann, J. Chem. Phys. **59**, 964 (1973).
[53]Z. H. Zhang, N. Abusalbi, M. Baer, D. J. Kouri, and J. Jellinek, in *Resonances in Electron-Molecule Scattering, van der Walls Complexes and Reactive Chemical Dynamics,* edited by D. J. Truhlar (American Chemical Society, Washington, D.C., 1984), p. 457.
[54]C. K. Lutrus and S. H. Suck Salk, Phys. Rev. A **39**, 391 (1989).
[55]W. M. Huo (unpublished).
[56]W. M. Huo and T. L. Gibson (unpublished).
[57]W. M. Huo and C. A. Weatherford (unpublished).